Acidic Ionic Liquids Enabling Intermediate Temperature Operation Fuel Cells

Hui Hou[a.b], Hanno Maria Schütz[c.d], Jürgen Giffin[a], Klaus Wippermann[a], Xinpei Gao[c.d], Alessandro Mariani[c.d], Stefano Passerini[c.d], Carsten Korte[a.b*]*

[a] Forschungszentrum Jülich GmbH, Institute of Energy and Climate Research, Electrochemical Process Engineering (IEK-14), 52425 Jülich, Germany

[b] Institute of Physical Chemistry, RWTH Aachen University, Germany

[c] Helmholtz Institute Ulm (HIU), Helmholtzstrasse 11, 89081 Ulm, Germany

[d] Karlsruhe Institute of Technology (KIT), P.O. Box 3640, 76021 Karlsruhe, Germany

Keyword: protic ionic liquid, fuel cell, Walden plot, oxygen reduction reaction, oxygen permeability

Abstract

Herein we show that protic ionic liquids (PILs) are promising electrolytes for fuel cells operating in the temperature range of 100–120 °C. N,N-diethyl-N-methyl-3-sulfopropan-1-ammonium hydrogen sulfate ([DEMSPA][HSA]), N,N-diethyl-N-methyl-3-sulfopropan-1-ammonium triflate ([DEMSPA][TfO]), N,N-diethyl-3-sulfopropan-1-ammonium hydrogen sulfate ([DESPA][HSA])

and N,N-diethyl-3-sulfopropan-1-ammonium triflate ([DESPA][TfO]) are investigated in this study with regard to their specific conductivity, thermal stability, viscosity and electrochemical properties. The [DEMSPA][TfO] and [DESPA][TfO] electrolytes offer high limiting current densities for the oxygen reduction reaction (ORR) on platinum electrodes, that is, about 1 order of magnitude larger than 98% H_3PO_4. This is explained by the minor poisoning of the Pt catalyst and the significantly larger product of the oxygen self-diffusion coefficient and concentration in these two PILs.

1. INTRODUCTION

Polymer electrolyte fuel cells (PEFCs) have attracted much interest in recent years because of the burgeoning electric transportation and as an alternative to rechargeable lithium batteries. The upscaling of a fuel cell system is rather simple since to double the capacity, only the hydrogen storage must be doubled. In the case of battery storage, doubling the capacity would practically require doubling the cell weight (*i.e.*, active electrode materials).

PEFCs employing sulfonated fluoropolymer membrane electrolytes (e.g., NAFION or AQUIVION) rely on the presence of water in the membrane to enable proton transfer between the two electrodes. This, however, restricts their operation below 80 °C (low temperature-PEFC, LT-PEFC), which, especially for small fuel cell systems, causes some challenges, such as (i) slow electrode kinetics, (ii) the need for a complex water management system, including feed gas humidification and water recirculation, (iii) inefficient cooling of the system arising from the meagre temperature difference between ambient and operating temperatures, (iv) poor reutilization of the waste heat, and (v) low tolerance against impurities in the feed gases. These issues, however, can be addressed by employing an electrolyte well conducting even above 100 °C. At such a temperature, in fact, the electrochemical kinetics for both electrode reactions are enhanced. Also,

no water recirculation and feed gas humidification would be required. The water produced in the reactions can leave the cell in the gas phase on the cathode side. Furthermore, tolerance against impurities (e.g., CO) increases considerably, as the poisoning effect of the redox catalyst (platinum, Pt) is temperature-sensitive.[1-3]

The use of phosphoric acid (H_3PO_4)-doped polybenzimidazole (PBI) membranes enables high temperature (HT-) PEFCs operation at 160–180 °C.[4] However, their widespread commercial application is impeded by their low power density due to the sluggish ORR kinetics. This is caused by phosphate species strongly adsorbing on the Pt catalyst and by poor oxygen solubility.[5]

Thus, a need exists for nonaqueous, proton-conducting electrolytes operating at intermediate temperatures (100–120 °C) enabling the realization of intermediate-temperature (IT-) PEFCs, avoiding the above-mentioned drawbacks of LT-PEFCs and HT-PEFCs.[6-7]

Protic ionic liquids (PILs) are promising nonaqueous electrolytes for operation at elevated temperatures because of their generally high thermal stability, wide electrochemical windows, good ionic conductivity, negligible vapor pressure, and nonflammability.[8-10] With regards to fuel cell applications in particular, the following criteria must be fulfilled by the electrolyte: (i) weak interaction between the electrolyte and the redox catalyst (Pt), (ii) an electrochemical window of at least from 1.3 to 0 V vs SHE, (iii) thermal stability up to at least 130 °C, (iv) good proton conductivity (e.g., 85 wt % H_3PO_4 has a conductivity of 0.55 S cm^{-1} at 150 °C),[11] and (v) high oxygen solubility and diffusivity in the electrolyte (e.g., in LT-PEFCs, water as an electrolyte has a c_{O_2} value of 9.4×10^{-7} mol cm^{-3} and a D_{O_2} of 3.3×10^{-5} cm^2 s^{-1} at 50 °C; in HT-PEFCs, H_3PO_4 has a c_{O_2} of 1.1×10^{-7} mol cm^{-3} and a D_{O_2} of 3×10^{-5} cm^2 s^{-1} at 150 °C).[12-14] When considering the oxygen permeability in NAFION 117 membrane, it achieves a D_{O_2} of 1.5×10^{-6} cm^2 s^{-1} and 4.9×10^{-6} cm^2 s^{-1} and a c_{O_2} of 8×10^{-7} mol cm^{-3} and 3.8×10^{-7} mol cm^{-3} at a temperature of 50 °C

and relative humidities of 50% and 95%, respectively.[15] The H_3PO_4-doped PBI polymer with a doping level of six shows a D_{O_2} of 1.9×10^{-6} cm^2 s^{-1} and 3.2×10^{-6} cm^2 s^{-1} and a c_{O_2} of 5.1×10^{-7} mol cm^{-3} and 6.8×10^{-7} mol cm^{-3} at a temperature of 150 °C and relative humidities of 1% and 10%, respectively.[16-17] When operating a fuel cell in an acidic electrolyte, the use of Pt (or Pt-based alloys) as the redox catalyst is inevitable, as no other metal catalysts are stable under these conditions.

An ionic liquid (IL) is defined as a salt with a melting point below 100 °C due to bulky (often organic) cations and anions, resulting in a low lattice energy. The threshold at 100 °C is an arbitrary definition.[18-19] In the case of a protic ionic liquid, the cation (or the anion) is a Brønsted acid, and thus it can act as a mobile proton carrier. A PIL with a cation carrying the proton can be synthesized by protonation of a Brønsted base with a Brønsted acid. The cation acidity of this type of PILs depends on the strength of the conjugated base (precursor of the cation). Over the past decade, several PILs have been investigated for potential PEFC applications. Most of these studies only focused on PILs with low acidic cations,[8, 20-25] *e.g.*, diethylmethylammonium triflate ([DEMA][TfO]) and bis(trifluoromethane sulfonyl)imide ([DEMA][TFSI]), dimethylaminoethyldimethylammonium triflate ([TEMEDA][TfO]) or benzimidazolium bis(trifluoromethane sulfonyl)imide ([BIM][TFSI]). The conjugated bases are very strong, which implies the high thermal stability of theses PILs. The ORR kinetics, oxygen solubility and diffusivity, and influence of the catalyst for the PILs ethylammonium nitrate ([EAN]), bis(2-methoxyethyl)ammonium benzoate ($[(MeOEt)_2NH][C_6H_5CO_2]$), sulfamate ($[(MeOEt)_2NH]$[OSA]) and acetate ($[(MeOEt)_2NH]$[Ac]) were investigated by Khan et al., while Noda et al. have determined the influences on the physicochemical and electrochemical properties when varying the base/acid stoichiometric ratio of imidazolium bis(trifluoromethane

sulfonyl)imide ([IM][TFSI]).[26-27] The ORR kinetics of a Pt surface by using [DEMA][TfO] as the electrolyte has been measured by Johnson et al.[28] It was found that even a trace of water (240 ppm) in [DEMA][TfO] is sufficient to cause the formation of PtO_x on the electrode surface at high potentials. The formation of the surface oxide layer is also influenced by the temperature; that is, the formed surface oxide increases with increasing temperature, hindering the ORR reaction.[28-29]

The various kinds of ionic liquids as the electrolytes immobilized in polymeric membranes for PEFC application have been published.[30-33] Lee et al. showed the feasibility of an intermediate temperature PEFC (100–140 °C) operated under nonhumidified conditions by using protic ionic liquids.[24] [DEMA][TfO] immobilized in a sulfonated polyimide polymer shows a sufficient thermal, mechanical stability and ionic conductivity. It exhibits a promising fuel cell performance under nonhumidified conditions.[24] Cloisite Na^+-sulfonated poly(2,5-benzimidazole) (ABPBI) composite membranes doped with ionic liquids (1-hexyl-3-methylimidazolium chloride, [HMIM][Cl], and 1,1,3,3-tetramethylguanidine tetrafluoroborate, [TMG][BF_4]) were prepared by Bao et al.[34] The highest ionic conductivity of 3.5×10^{-3} S cm^{-1} is achieved at 120 °C for the [HMIM][Cl]-doped composite membrane. In the case of the [TMG][BF_4]-doped membrane a value of 2.1×10^{-3} S cm^{-1} can be reached.[34] The feasibility of novel membranes based on the ionic liquid 1-methyl-3-propyl-methylimidazolium dihydrogen phosphate ($PMIH_2PO_4$), PBI as a host polymer, and additional H_3PO_4 applied in fuel cells was published by Ye et al.[35] The maximum conductivity at 120 °C for the H_3PO_4/$PMIH_2PO_4$/PBI composite membrane has a value in the order of 10^{-3} S cm^{-1} under anhydrous conditions.[35]

Taking a different approach, in this study PILs with highly Brønsted acidic cations were investigated. A zwitterionic compound with a sulfonic acid group is chosen as a very weak base, while the anions triflate and hydrogen sulfate are used. In particular, the physicochemical and

electrochemical properties of the four PILs–N,N-diethyl-N-methyl-3-sulfopropan-1-ammonium hydrogen sulfate ([DEMSPA][HSA]), N,N-diethyl-N-methyl-3-sulfopropan-1-ammonium triflate ([DEMSPA][TfO]), N,N-diethyl-3-sulfopropan-1-ammonium hydrogen sulfate ([DESPA][HSA]), and N,N-diethyl-3-sulfopropan-1-ammonium triflate ([DESPA][TfO])–are investigated. In a fuel cell the electrode reactions include the anodic hydrogen oxidation (HOR) and the cathodic oxygen reduction (ORR). The HOR has generally a much faster kinetics and thus a significantly lower overpotential compared to ORR. As known from investigations using aqueous electrolytes, the ORR has a much more complex reaction mechanism than the HOR. A break of the strong O=O bond is necessary and a consecutive transfer of four electrons (HOR: only two electron transfers).[36] The HOR kinetics is at least 6 orders of magnitude faster than the ORR kinetics in a state-of-the-art H_2/air PEFC with Pt catalysts.[37-38] Thus, the ORR performance of the four PILs is focused on in this work.

2. EXPERIMENTAL SECTION

2.1 PILs Preparation

All chemicals were used as received. The PILs were synthesized and stored under a nitrogen atmosphere considering their strong hygroscopicity. Diethylamine (3.76 g, ≥99.5%, Sigma-Aldrich) and 1,3-propane sultone (6.3 g, 99%, Alfa Aesar) were dissolved in acetone (20 g, 20 g) separately. Acetone was used as common solvent enabling the reactants mixing sufficiently and meanwhile slowing down the reaction rate. The 1,3-propane sultone/acetone solution was dropped slowly into the diethylamine/acetone solution. The reactants were stirred in an ice bath for 3 h and then stirred at room temperature for 3 days. The precipitate, N,N-diethyl-3-aminopropane-1-sulfonic acid, was filtered, washed with acetone several times, and dried at 80 °C under vacuum. [DESPA][HSA] and [DESPA][TfO] were prepared by mixing the zwitterionic base (5.02 g) with

an equimolar amount of the acids (2.51 g, sulfuric acid, ≥98%, Merck; 3.84 g, triflic acid, reagent grade, 98%, Sigma-Aldrich) at 80 °C for 1 h. A schematic of synthesis procedure is shown in Figure 1. Using N,N-diethyl-N-methylamine (4.24 g, 98%, ACROS Organics) and 1,3-propane sultone (5.88 g) as reactants, 3-(diethyl(methyl)ammonium)propane-1-sulfonate was synthesized with a similar procedure. [DEMSPA][TfO] and [DEMSPA][HSA] were prepared as described above. The molar fraction of (residual) water in the samples was adjusted to a similar value. To characterize the electrochemical properties of the new highly acidic PILs for fuel cell operation, a molar fraction of 0.25 ± 0.04 H_2O was chosen. This corresponds to 1.3–2.05 wt %. The stationary water content in a future PEFC suitable for 120 °C operation can only be estimated, as it depends on various parameters like operation temperature, pressure, and volume flow of the H_2/air inlet/outlet. Taking experimental results from HT-PEFC operation at 160 °C into account (H_2O molar fraction of 0.05–0.18 at the outlet of the cathode and anode), a water content in the order of 1–2 wt % is a first (but conservative) approximation.[39]

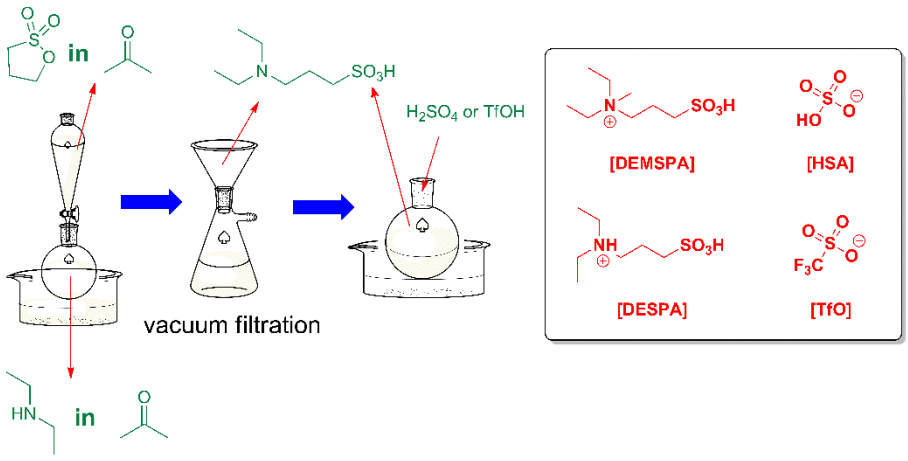

Figure 1. Schematic drawing of the PIL [DESPA][HSA] or [DESPA][TfO] preparation and the structure of the cations [DEMSPA] and [DESPA] as well as anions [HSA] and [TfO].

2.2 Physical/Thermal Characterization and Ionic Conductivity

The water content of the PILs was determined by means of Karl Fischer titration (C30 coulometric KF titrator, Mettler Toledo or 825 KF Titrando, Metrohm). The density measurements were performed by using an oscillating U-tube density meter (Anton-Paar DMA 4100M). The viscosity was measured with a rheometer (Anton-Paar MCR102) by using the cone-plate geometry (cone and plate were PTFE-coated). The sample was measured from 30 to 80 °C with a temperature interval of 10 °C, following by measuring from 80 to 30 °C. The change of the water content in the samples before and after the measurements was rather minor, as the difference in the measured values for ascending and descending temperatures was only small. The standard deviation is shown in Figure S1. The constant shear rate was set at 20 s^{-1} to ensure Newtonian behavior. The integration time of 3 s and the equilibrated time of 15 min at each temperature were used. The average value was adopted as measured viscosity. The density and viscosity measurements were performed in a dry room (dew point: -70 °C). The dynamic thermal behavior was examined in an open quartz glass crucible from 100 to 500 °C at a heating rate of 10 K min^{-1} under a N_2 atmosphere by using a PerkinElmer STA 6000 device. Isothermal TG experiments were performed by using a TG 209 F1 Libra (Netzsch) with a purge of a gas mixture close to synthetic air composition, obtained by the injection of 7 mL min^{-1} O_2 and 33 mL min^{-1} N_2. The thermobalance was protected by a 20 mL min^{-1} flow of N_2. Samples were only handled inside the dry room to prevent water uptake from the environment. All samples were freshly prepared before the isothermal TG measurement to exclude alterations during storage. The water content was gravimetrically adjusted to be comparable with the other samples. Samples with a weight of 2.1 ± 0.1 mg were sealed in hermetic aluminum crucibles (DSC-crucibles, 25 µL Netzsch) and inserted in the TG furnace. The lids were pierced by the autosampler (Netzsch) prior the measurement. The differential scanning calorimetry

(DSC) measurements were performed between -140 and 80 °C at a rate of 5 K min^{-1} by using a TA Instruments Q2000 equipped with a liquid N_2 cooling system. The samples were sealed hermetically in pretreated Al pans. The Al pans were preheated to 550 °C for 2 h under an air atmosphere to oxidize the surface.

The ionic conductivity of the PILs was determined by a conductometer performing the measurements at several frequencies (MMates Italia). The samples were sealed in glass conductivity cells with two platinized platinum electrodes. The cell constant was determined by using a 0.01 M KCl solution as a standard. The cells were heated from 30 to 120 °C and then cooled to 30 °C by using a thermostatic bath. After each temperature step, the samples were equilibrated for 50 min. The data were recorded every 30 s, and the averaged value was employed. The standard deviations are within 0.01 mS cm^{-1}.

2.3 ORR Kinetics

The in-house-designed setup used for the electrochemical measurements is described in detail by Wippermann et al.[20] Briefly, a Pt crucible (99.9% purity, m&k GmbH) with the shape of a truncated cone and a volume of 4–5 ml was used as the counter electrode (CE) and testing cell. The working electrode (WE) was made of a Pt wire (1 mm diameter, 78 mm length; 99.9%, MaTeck Material Technologie & Kristalle GmbH) fused into a glass tube. The WE was polished by using SiC 2000 and SiC 4000 abrasive paper and 0.3 and 0.05 μm alumina suspension (Allied High Tech Products). The polishing was followed by an ultrasound cleaning at room temperature for 30 min. A roughness factor of 1.4 was determined by cyclic voltammetry using 0.5 M H_2SO_4 (96%, Merck) and an actual electrode surface of the WE is 0.301 cm^2. A hydrogen-saturated palladium electrode (Pd-H electrode) was employed as the reference electrode (RE), having a fixed potential of 50 mV vs RHE at 25 °C. A palladium wire (1 mm diameter; 99.95%, MaTeck Material Technologie &

Kristalle GmbH) with a round polished tip was used. The temperature dependence of the Pd-H electrode potential in the range of 30–130 °C in highly acidic solutions like 95 wt % H_3PO_4 and 95 wt % 2-sulfethylammonium triflate [2-SEA][TfO] (an analogue PIL) was determined by Wippermann et al. The Pd-H potential vs RHE shows a linear increase with the cell temperature.[20] All electrochemical measurements were processed by using a potentiostat/impedance analyzer (Zennium electrochemical workstation, ZAHNER Elektrik GmbH).

The ORR kinetics of the PILs was investigated by recording the polarization curves using the described three-electrode setup. The curves were recorded in the temperature range of 90–120 °C with a scan rate of 5 mV s^{-1}. The PILs were saturated with oxygen at a flow rate of 20 mL min^{-1} for 2 h. The volume flow rate was adjusted with a mass flow controller (Brooks Instruments). The cell's temperature was controlled by using a cryostat (Lauda kryothermostat ECO RE415) with the heat transfer oil circulated in a heating jacket.

The measured (cathodic) current density, j, consists of a kinetic current density, j_k, corresponding to the ORR kinetics and a limiting diffusion current density, j_d, due to the diffusional mass transfer in vicinity of the electrode surface. Provided that j_k and j_d are independent of each other, they can be separated by means of the Koutecký-Levich equation:

$$\frac{1}{j} = \frac{1}{j_k} + \frac{1}{j_d} \tag{1}$$

The kinetic current density j_k, the apparent factor b_{app}, and the intrinsic factor b_{int} are calculated via eqs 2–4 as follows: [20, 40-43]

$$\log j_k = \log \frac{j_d j}{j_d - j} \tag{2}$$

$$\frac{d(\log j_k)}{d(U_0 - U)} = \frac{1}{b_{app}} = \frac{1}{b_{int}} + \frac{1}{1-\theta_{ox}} \frac{d\theta_{ox}}{dU} \tag{3}$$

$$b_{int} = \frac{2.3026\, RT}{\beta_c F} \tag{4}$$

where the cell potential is denoted with U and the OCV potential with U_0, θ_{ox} is a term related to the change of the surface coverage by the chemisorbed oxygen, and β_c is the (cathodic) symmetry factor.

2.4 Chronoamperometry Measurement, Oxygen Diffusivity, and Solubility

The oxygen diffusion coefficient D_{O_2} and oxygen saturation concentration c_{O_2} of the PILs were determined by potential-step chronoamperometry using the same setup described above but employing a working circular and flat microelectrode prepared by using a Pt wire (250 µm diameter; 99.9%, MaTeck Material Technologie & Kristalle GmbH) fused into a glass jacket. To remove impurities on the electrode surface, the WE was polished following the procedure described above. A roughness factor of 1.3 was determined with the same method illustrated above. After equilibration at OCV, an appropriate cell potential forcing the ORR diffusion limitation to occur was applied.[27] The oxygen diffusion coefficient and saturation concentration were calculated by fitting the temporal evolution of the cell current to the Shoup-Szabo equation: [10, 44]

$$I = -4n\mathrm{F}Drc\ \mathrm{f}(\tau) \tag{5}$$

$$\mathrm{f}(\tau) = \frac{\pi}{4} + \frac{\pi^{1/2}}{2\tau^{1/2}} + 0.2146e^{-0.7823\tau^{-0.5}} \tag{6}$$

$$\tau = \frac{4Dt}{r^2} \tag{7}$$

The number of electrons is denoted with n, the Faraday constant with F, the elapsed time with t, and the radius of the electrode with r. In the case of the Shoup-Szabo equation, an ideal planar circular electrode surface and a semi-infinite diffusion space are assumed. The nonlinear curve fitting was performed by using the software OriginPro 2019 (Originlab Corp.).

2.5 Linear Sweep Voltammograms and Electrochemical Stability

Linear sweep voltammograms (LSVs) were performed at 120 °C in a N_2-saturated atmosphere with a scan rate of 2 mV s^{-1}. The setup for the measurement is described in subsection 2.3.

3. RESULTS AND DISCUSSION

3.1 Thermal Analysis

The dynamic TG curves and their DTG curves of the four fresh prepared PILs are depicted in Figure 2a. The samples were pretreated at 100 °C for 20 min to reduce the residue water content. The decomposition temperature of the PILs is the temperature corresponding to the first peak shown in the DTG curve. The thermal stability increases with the following order: [DESPA][HSA] < [DEMSPA][HSA] < [DEMSPA][TfO] < [DESPA][TfO].

To investigate the thermal stability of the PILs under IT-PEFC operando conditions, isothermal TGA experiments in the presence of oxygen were performed (Figure 2b). The heating protocol used consisted of an initial isothermal step of 6 h at 100 °C, followed by 2 h steps at 120, 130, 150, 180, and, finally, 200 °C. The PILs expect the [DEMSPA][HSA] show a weight loss of 3.4–5.6 wt % at 100 °C for 6 h. This exceeds of the original water contents (i.e., about 2 wt %) in PILs but still in the acceptable range. With regard to on the [DEMSPA][HSA], a weight loss of 10 wt % is observed. The formation of volatile complexes between water and sulfuric acid explains the observed mass losses. Thus, [DEMSPA][HSA] is not the best candidate for the IT-PEFC application. For all PILs in Figure 2b, besides [DEMSPA][TfO], the TG curve gets steeper during the isothermal steps at 150 and 180 °C. The slope change is undoubtedly an indication of the decomposition onset in this temperature range. Based on this observation, [DEMSPA][TfO] seems to be the most stable PIL of the investigated series. The stability found in the isothermal run is slightly different compared to the dynamic scan. A reasonable explanation should consider the different protocols used for the two measurements, with a pivotal role played by the gas used to purge the samples (inert N_2 or N_2/O_2 mixture).

The DSC thermal analysis was performed in the temperature range between −140 °C (133 K) and 80 °C (353 K). Neither crystallization nor melting peaks were observed; however, all PILs showed a glass transition around −53 °C (220 K), as shown in Figure 2c.

The glass transition temperature of PILs is seen to depend on the geometry of cations and anions (steric effects), their mutual Coulomb and H-bond interactions, and the presence of residual water.[45] The PILs with the more voluminous [DEMSPA] cation exhibit glass transition temperatures about 2 K higher than the [DESPA]-based PILs. This indicates lower interionic and intermolecular interaction energies for the [DESPA]-based PILs and thus a higher ion mobility and disorder. Also, the glass transition of the [TfO]-based PILs is about 3 K lower than that of the [HSA]-based counterparts. This indicates increased interionic and intermolecular interactions when [HSA] anions are present, which may be caused by a higher average number of H bonds between the anions and cations.

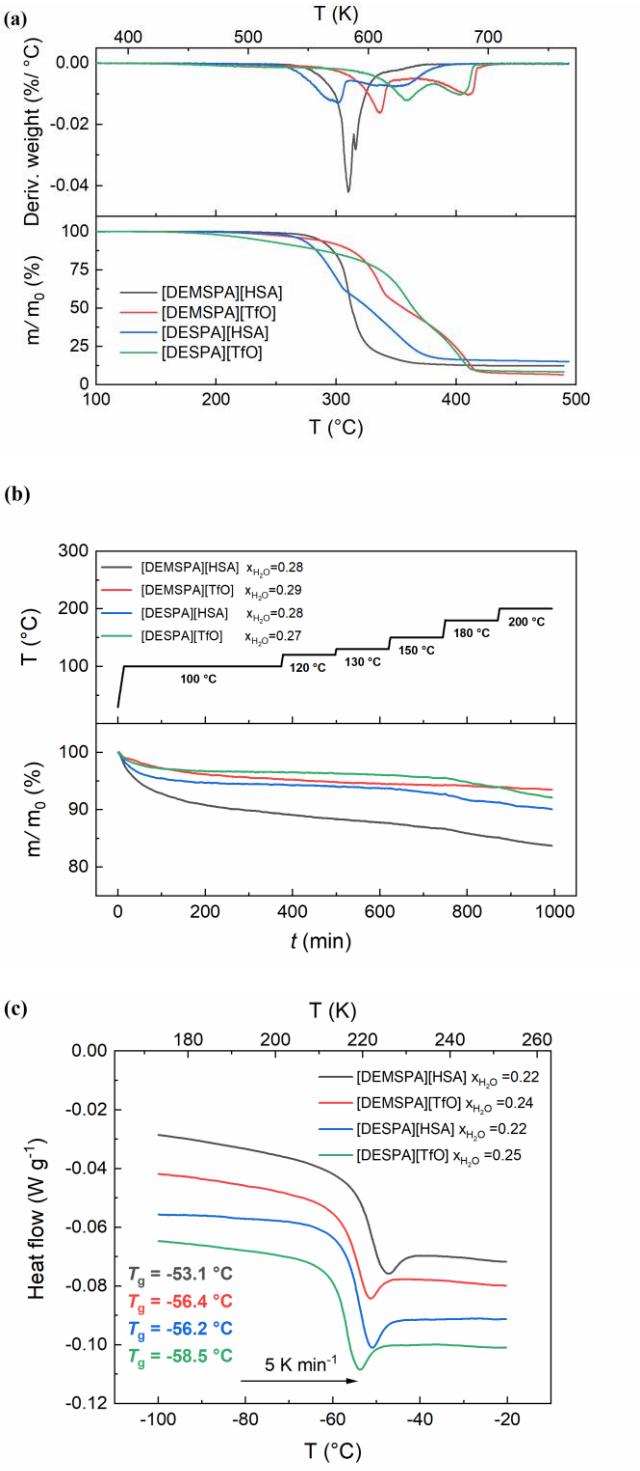

Figure 2. (a) Dynamic TG curves and DTG curves of the investigated PILs at a heating rate is 10 K min^{-1} under a N_2 atmosphere. The samples were pretreated at 100 °C for 20 min to reduce their water contents. (b) Isothermal TG of PILs. The measurements were performed with a flow of

7 mL min^{-1} O_2 and 33 mL min^{-1} N_2. The scan rate between the steps was 5 K min^{-1}, and the initial water molar fractions were adjusted to 0.27–0.29. (c) DSC heating traces of PILs with a heating or cooling rate of 5 K min^{-1}. The traces are shifted vertically for clarity.

3.2 Density

The density of all investigated PILs decreases with increasing temperature (see Figure 3), as it can be expected due to thermal expansion. In the investigated temperature (30–80 °C, 303–353 K) a quasi-linear dependence is found. At room temperature, the PILs with the most voluminous, sterically hindered [DEMSPA] cation show a roughly 1% lower density than those with the [DESPA] cation. This trend agrees well with those reported by Gardas et al.; that is, the density is smaller in 1-butyl-2,3-dimethylimidazolium hexafluorophosphate ([BMMIM][PF_6]) than in 1-butyl-3-methylimidazolium hexafluorophosphate ([BMIM][PF_6]) because of a new substitution in the cation present.[46-47] Upon comparison of the PILs with the [TfO] anion to those with the [HSA] anion, the density is about 2% higher. This difference is simply explained by the fact that [TfO] is significantly heavier than [HSA] but not significantly larger.

To characterize the thermophysical properties of the PILs, *i.e.*, temperature dependence of the volume variation at constant pressure, the isobaric thermal expansivity α_p is defined, as per eq 8:

$$\alpha_p = -\frac{1}{\rho}\left(\frac{\partial \rho}{\partial T}\right)_P \tag{8}$$

α_p is positive at ambient pressure for all investigated PILs (see Figure 3), indicating a volume expansion upon increasing temperatures. However, [TfO]-based PILs seem to expand more markedly than [HSA]-based PILs because of the weaker hydrogen bonds triflate is forming. It is in fact known that [TfO] is a weakly coordinating anion, which loosely interacts with cations. The fact that α_p values increase with increasing temperature indicates a deviation from linearity in the temperature dependency of density for the studied PILs.

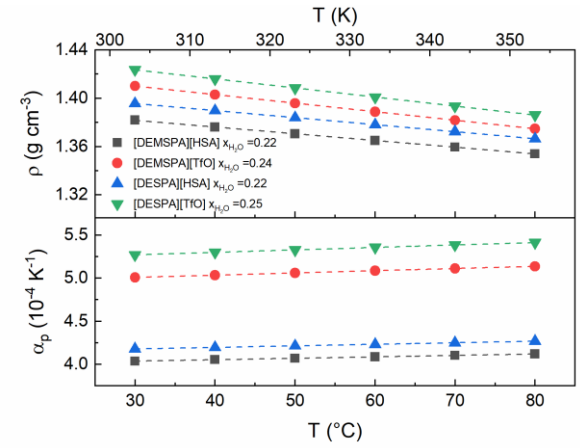

Figure 3. Isobaric thermal expansivity α_p against temperature and the temperature dependence of the density in PILs.

3.3 Dynamic Viscosity and Conductivity

The dynamic viscosity and the specific conductivity of all investigated PILs exhibit a Vogel-Fulcher-Tammann behavior (VFT) as a function of temperature, as per eq 9:

$$\zeta = \zeta_0 \exp\left[\frac{B_\zeta}{\mathrm{R}(T-T_{0\zeta})}\right] \tag{9}$$

Here, ζ is alternatively the dynamic viscosity η or specific conductivity σ. The modulus of B_ζ is the pseudo-activation energy for the viscous flow or ionic transport, $T_{0\zeta}$ is termed the temperature of zero configurational entropy and correlated to the glass transition temperature, R is the gas constant, and ζ_0 is the pre-exponential factor.[48-50] The VFT fitting parameters of the viscosity and conductivity data in the investigated temperature range (30–80 °C and 30–120 °C, respectively), the absolute values of B_η, B_σ and $T_{0\eta}$, $T_{0\sigma}$ are listed in Table 1. The viscosity vs $1000(T - T_{0\eta})^{-1}$ and the conductivity vs $1000(T - T_{0\sigma})^{-1}$ are depicted in Figures 4a and 4b, respectively. The VFT fitting of the dynamic viscosity and conductivity are shown in Figures S1 and S3.

The viscosity data and the specific conductivity data can also be interpreted by the Arrhenius rule:

$$\eta = \eta_0 \exp\left(-\frac{E_a}{RT}\right) \quad (10)$$

$$\sigma = \frac{\sigma_0}{T} \exp\left(-\frac{E_a}{RT}\right) \quad (11)$$

However, there is no simple Arrhenius-Andrade behavior with constant activation energy, E_a. Fitting the temperature-dependent viscosity data to eq 10 would lead to systematic deviations (see Figure S2). Thus, the free volume change with increasing temperature dominates the viscous behavior of the PILs. Those containing the [DEMSPA] cation generally show higher viscosity than the corresponding PILs with the [DESPA] cation. When comparing PILs with the same cation, the higher viscosity is observed for the [HSA] anion. Thus, [DEMSPA][HSA] shows the highest viscosity among all PILs, which decreases from 67.2 Pa s at 30 °C (303 K) to 1.8 Pa s at 80 °C (353 K). Instead, the lowest viscosity is observed for [DESPA][TfO], which value decreases from 5.3 to 0.3 Pa s within the same temperature interval. The pseudo-activation energy, $|B_\eta|$, increases in the order [DESPA][TfO] < [DESPA][HSA] ≈ [DEMSPA][TfO] < [DEMSPA][HSA] by about 54%.

The specific conductivity data show no simple Arrhenius behavior with a constant activation energy, E_a, as given in eq 11, (see Figure S4), implying that the change in the free volume with increasing temperature also dominates ionic transport in these PILs. The highest conductivities can be found for the PILs based on the [DESPA] cation. Upon comparison of the PILs with the [TfO] anion to those with the [HSA] anion, the latter exhibit higher conductivities. In fact, the highest conductivities are found for [DESPA][HSA] (0.15 mS cm^{-1} at 30 °C and 7.22 mS cm^{-1} at 120 °C). The absolute value of the pseudo-activation energy, B_σ, for conductivity increases in the order [DESPA][TfO] < [DEMSPA][TfO] ≈ [DESPA][HSA] < [DEMSPA][HSA]. However, the change

is about 27%; that is, only half of the change compared to the pseudo-activation energy $|B_\eta|$ of the viscous flow.

The proton conductivity includes contribution from a vehicular and–depending on the H_2O content–from a cooperative transport mechanism. In the analogue PIL 2-sulfethylmethylammonium triflate ([2-SEMA][TfO]), cation and anion exhibit a comparable mobility in the neat compound without water.[51] This results in a transference number for H^+ transport of about 1/2, *i.e.*, if only vehicular H^+ transport is possible. An increasing water content will also increase the concentration of H_3O^+ due to the protolysis equilibrium with the high acidic PIL cations. The H_3O^+ cations can act in a vehicular mechanism as another (presumably more) mobile protonic charge carriers in the PIL but it could also result in a cooperative proton transfer by fast proton exchange processes with the free base, the PIL cation and water.[51] Both may be the origin of the observed sharp increase of the proton mobility of about 1 order of magnitude.

Table 1. VFT Fitting Value of Pseudo-Activation Energies $\boldsymbol{B_\eta}$ and $\boldsymbol{B_\sigma}$ and the Characteristic Temperatures $\boldsymbol{T_0}$

PILs	viscosity η		(total) conductivity σ	
	$\lvert B_\eta \rvert$ (kJ mol^{-1})	$T_{0\eta}$ (K)	$\lvert B_\sigma \rvert$ (kJ mol^{-1})	$T_{0\sigma}$ (K)
[DEMSPA][HSA]	8.5 ± 0.3	147.0 ± 3.0	5.7 ± 0.1	163.8 ± 2.1
[DEMSPA][TfO]	6.3 ± 0.2	164.9 ± 1.8	4.9 ± 0.1	179.1 ± 2.2
[DESPA][HSA]	6.2 ± 0.2	160.2 ± 2.2	5.0 ± 0.1	162.8 ± 1.6
[DESPA][TfO]	5.5 ± 0.1	167.5 ± 1.0	4.5 ± 0.1	176.0 ± 1.5

Parameters obtained from the temperature-dependent viscosity and (total) conductivity data of the PILs. The depicted uncertainty was obtained from the fitting.

When the microscopic processes for ionic transport are directly coupled to microscopic viscous flow, their absolute values of the pseudo-activation energies $|B_\sigma|$ and $|B_\eta|$ should (ideally) be equal.

For an electrolyte with i mobile ionic charge carriers, this would result in the well-known Walden rule:

$$\Lambda\eta = \frac{e^2 N_A}{6\pi}\sum_i \frac{z_i^2 \nu_i}{r_i}\alpha_{\mathrm{Diss}} = \mathrm{const.} \quad \text{with} \quad \Lambda = \sum_i \nu_i \lambda_i \tag{12}$$

Here, Λ denotes the total molar conductivity, z_i and ν_i are the charge number and stoichiometric coefficient of each mobile ionic carrier, and r_i its hydrodynamic radius. The degree of dissociation of the electrolyte is given by α_{Diss}. The total molar conductivity Λ depends on the partial molar conductivities λ_i of all mobile charge carriers i. If the total electrolyte concentration is given as c_0 and the concentration of each mobile charge carrier as c_i, they can be calculated as:

$$\Lambda = \frac{\sum_i \sigma_i}{c_0} \quad \text{and} \quad \lambda_i = \frac{\sigma_i}{c_i} \quad \text{with} \quad c_i = \nu_i c_0 \alpha_{\mathrm{Diss}} \tag{13}$$

However, the decoupling of the ionic charge and viscous transports may occur due to an intermolecular cooperative mechanism. In such a case, the relationship between molar conductivity and dynamic viscosity is modified and given by the fractional Walden rule:

$$\Lambda\,\eta^{\alpha} = \mathrm{const.} \tag{14}$$

The exponent α describes the extent of decoupling between ionic conduction and viscous flow, *i.e.*, $\alpha = |B_\sigma / B_\eta|$. Plotting the logarithm of the total conductivity, Λ vs that of the fluidity, η^{-1}, should yield a linear dependence with a slope equal to exponent α: [52]

$$\log\Lambda = \log \mathrm{C} + \alpha \log \eta^{-1} \tag{15}$$

In an aqueous 1 M KCl solution, full dissociation ($\alpha_{\mathrm{Diss}} = 1$) and pure vehicular charge transport mechanism ($\alpha = 1$) occur, yielding to a linear relationship with a slope of 1 in the Walden plot. The constant C is equal to the right side of eq 12. When the units 0.1 Pa s (≡ P, poise) are used for the dynamic viscosity and S cm^2 mol^{-1} for the molar conductivity, the data points for the aqueous KCl–the "KCl line"–will hit the origin of the plot.

Generally, the Walden plot gives a qualitative assessment tool for ionicity of the PILs. However, the ion size is not taken into consideration, which is certainly an influence factor. In this case, MacFarlane et al. proposed to include the ion size correction in the Walden rule offering the more explicit assessment to PIL ionicity: [53]

$$\log\Lambda = \log \mathrm{C}' + \alpha \log\ [\left(\frac{1}{r^+} + \frac{1}{r^-}\right)\eta^{-1}] \qquad (16)$$

where r^+ and r^- are the radius correction of the cations and anions for Walden plots obtained from atomic and bond contributions of the van der Waals volume (VABC).[54-55] This approach proved to work well with protic ionic liquid system.[56] The Walden plot (see Figure S5) and the adjusted Walden plot (see Figure 4c) are depicted. The adjustment influences significantly on the distances of all PILs to the ideal KCl line (Table 2). This adjustment has a similar effect to create a new reference line for the PILs, but it brings the advantage in assessing the ionicity of the PILs. [HSA]-based PILs are near the ideal KCl line, suggesting a high ionicity. In the PILs with [TfO] anions, the exponent α does not differ much from unity (see Table 2). This is not surprising, as the pseudo-activation energies $|B_\eta|$ and $|B_\sigma|$ are relatively close (see Table 1). As the exponent α indicates a decoupling between ionic transport and viscous flow, the H^+ transport in the [TfO]-based PILs may be dominated by a vehicular mechanism. The proton transport in the [HSA]-based PILs may include a contribution from a cooperative mechanism as the slope deviates slightly more from one.

Table 2. Radius Correction of the Cations and Anions for Walden Plots and Axis Intercepts C and C′ as Well as Exponent α Obtained from Original and Adjusted Walden Plots of the PILs

PILs	r^+ (Å)	r^- (Å)	log C	adjusted log C′	α
[DEMSPA][HSA]	3.65	2.44	-1.27	-0.30	0.83
[DEMSPA][TfO]	3.65	2.76	-1.91	-0.80	0.93
[DESPA][HSA]	3.55	2.44	-1.35	-0.37	0.84
[DESPA][TfO]	3.55	2.76	-1.89	-0.80	0.92

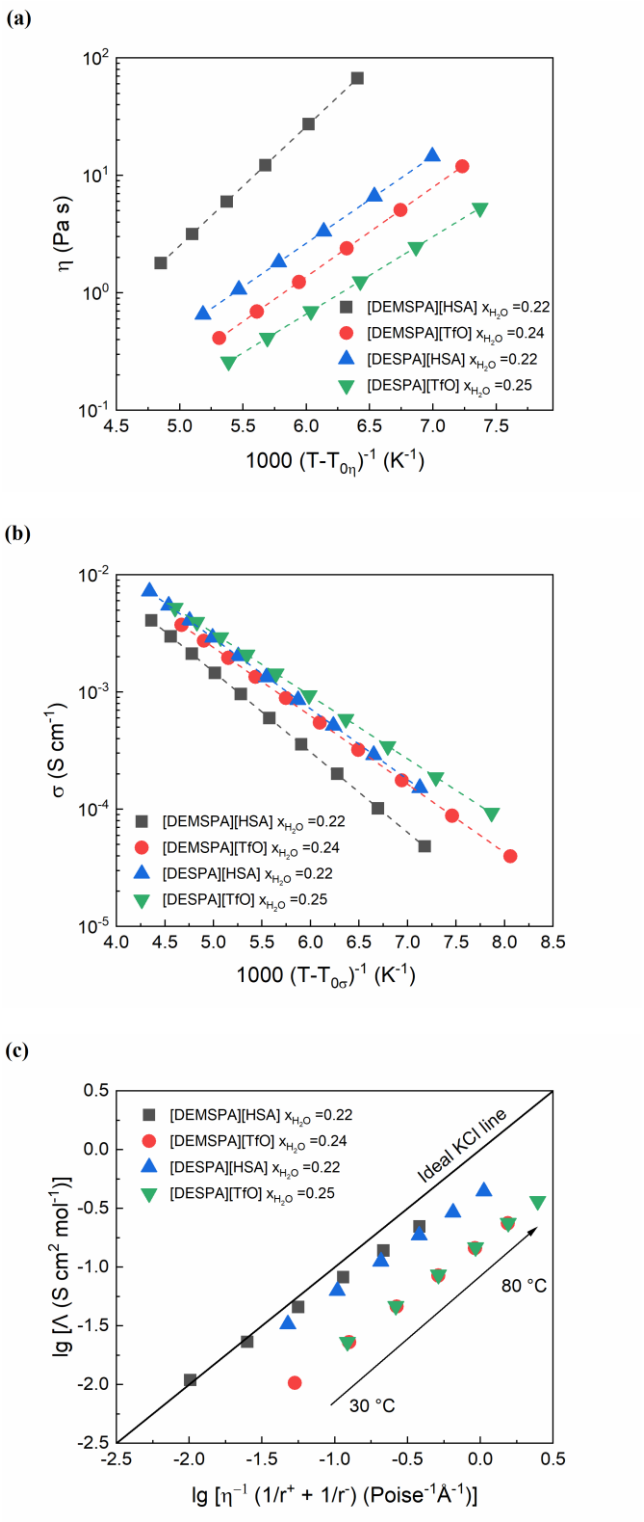

Figure 4. (a) Dynamic viscosity vs $1000(T - T_{0\eta})^{-1}$ of the PILs. (b) Specific conductivity vs $1000(T - T_{0\sigma})^{-1}$ of PILs. The symbols represent the experimental data, and the broken lines correspond to

the linear fitting, with $R^2 \geq 0.9999$. (c) Adjusted Walden plot of the PILs. The molar conductivity is calculated from the total conductivity considering the water fraction of the investigated PILs. The molar conductivity and viscosity are measured in the temperature range of 30–80 °C and the straight line is the correlated ideal Walden line (1 M KCl aqueous solution).

3.4 Electrochemical Stability of PILs

The electrochemical stability of the PILs was investigated by linear sweep voltammetry (LSV) (see Figure 5). Obviously, neither oxidation nor reduction of the [TfO]-based PILs takes place in the potential range between hydrogen and oxygen evolution; that is, the electrochemical window is solely determined by the electrochemical stability of the water. The [HSA]-based PILs show the narrow electrochemical windows compared to [TfO]-based PILs. Thus, the [TfO]-based PILs herein investigated appear to be more suitable for the operation of PEFCs.

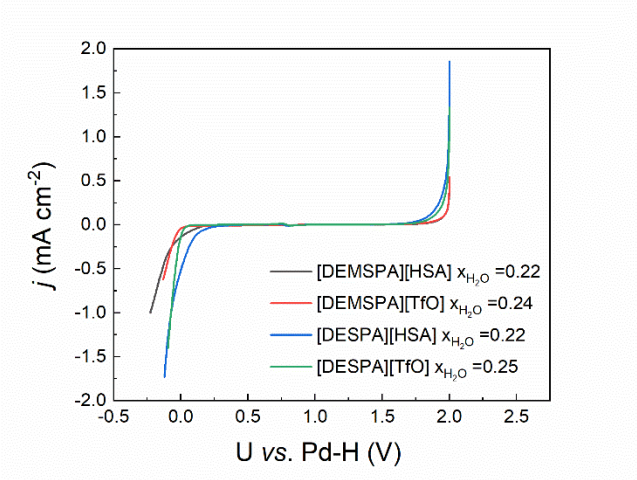

Figure 5. Linear sweep voltammograms of PILs performed at 120 °C with a scan rate of 2 mV s^{-1}.

3.5 Oxygen Solubility and Diffusivity

To obtain a mechanically stable electrolyte membrane for use in a PEFC, the electrolyte (PIL) must be immobilized in a host polymer matrix. The electrochemical contact between the electrolyte

membrane and the platinum-based redox catalyst in the porous electrode structure is established by a thin film of PIL, spreading from the membrane. The total ORR kinetics also depend on the O_2 transport rate in the PILs, as O_2 must pass through the liquid phase to reach the catalyst particle surface. Thus, the (equilibrium) solubility c_{O_2} and diffusivity D_{O_2} of oxygen in the PILs are crucial parameters in ORR kinetics.

For the chronoamperometry investigation of the PILs, a potential jump is applied to the cell from the OCV to a value where the diffusional current limitation for the ORR is reached. The data recorded at first 20 ms are discarded to minimize the current influence on the charging of the electric double layer.[57] The oxygen diffusion coefficient D_{O_2} and solubility c_{O_2} were evaluated by fitting the current vs time response curves by using the Shoup-Szabo equation (see eq 5–7). The diffusion coefficients D_{O_2} and (saturation) concentrations c_{O_2} in the temperature range of 90–120 °C are compiled in Figure 6a–c for all investigated PILs. All systems show acceptable reproducibility.

The oxygen diffusion coefficients, D_{O_2}, of the investigated PILs in the temperature range of 90–110 °C are all on the same order of magnitude (10^{-5}–10^{-6} cm^2 s^{-1}) of those found for 98% H_3PO_4 (see Figure 6a). On the other hand, the oxygen saturation concentrations, c_{O_2}, are about 1 order of magnitude higher (10^{-6}–10^{-7} mol cm^{-3}) than those of 98% H_3PO_4 (see Figure 6b).[14] The [TfO]-based PILs show a higher oxygen solubility than [HSA]-based PILs. This may explain by the enhanced oxygen solubility in fluorinated solvents.[58]

For the [HSA]-based PILs, the oxygen diffusion coefficients increases with temperature across the entire investigated range. However, the [TfO]-based PILs show a maximum of about 110 °C, although these findings may only have limited validity because of the limited number of data

points. A general trend for oxygen solubility with increasing temperature is hard to conclude. There is a debate on the oxygen solubility–temperature dependence in many published works.[10, 27, 59-62]

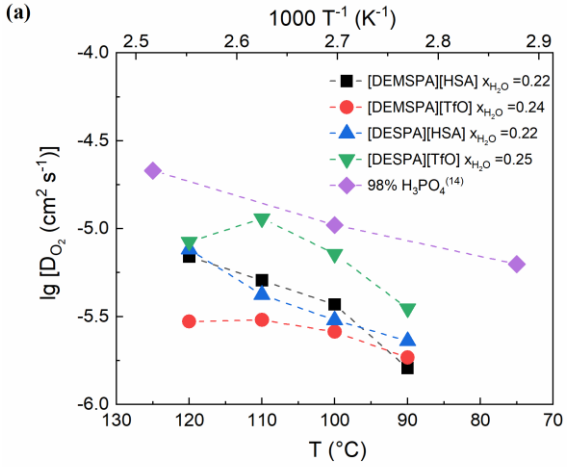

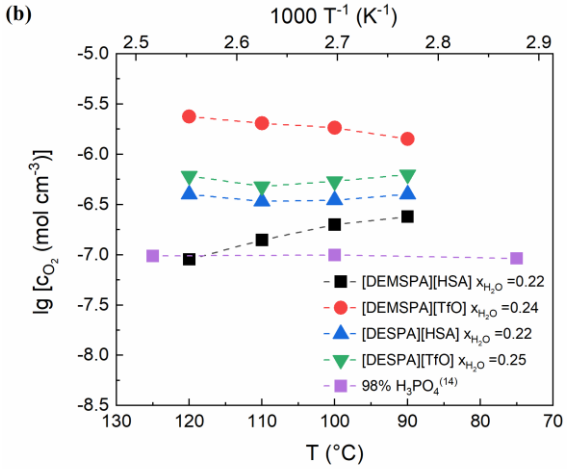

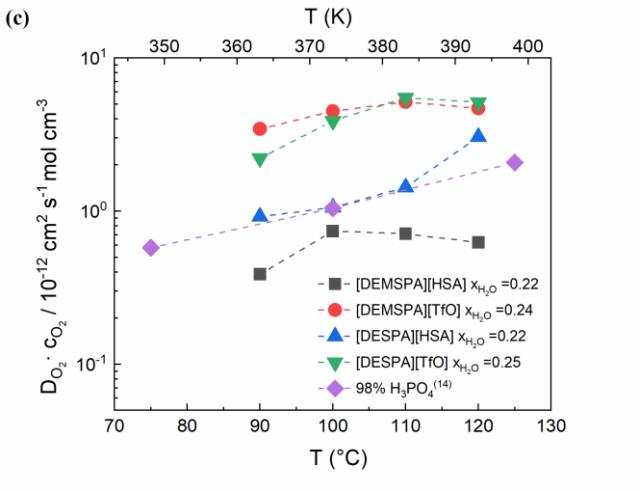

Figure 6. (a) Oxygen diffusion coefficient ($\boldsymbol{D}_{O_2}$), (b) solubility ($\mathbf{c_{O_2}}$), and (c) their product ($\boldsymbol{D}_{O_2} \cdot \mathbf{c_{O_2}}$) vs *T* in PILs and in 98% H_3PO_4.[14] The lines are only intended to be a guide for the eye.

3.6 ORR Kinetics

The ORR current density *j* of a Pt electrode recorded by using various PILs was measured in the temperature range of 90–120 °C (363–393 K). Before starting the voltage sweep to record the ORR current, we saturated the PIL with oxygen. According to the literature, the ORR on a Pt catalyst in acidic nonaqueous electrolytes follows most probably also a four-electron mechanism. This has been confirmed not only for 85 wt % H_3PO_4 but also for the protic ionic liquids [2-SEA][TfO], [DEMA][TfO], and [2-SEMA][TfO].[20, 63-65]

The quasi-stationary cathodic (ORR) polarization curves in the temperature range of 90–120 °C (363–393 K) of the electrolytes [DEMSPA][TfO] and [DESPA][TfO] are depicted in Figure 7a and of [DEMSPA][HSA] and [DESPA][HSA] in Figure 7c. The current density *j* was recorded by sweeping the potential with a scan rate of 5 mV s^{-1} in the negative direction from the OCV to values where the diffusional current limitation is observed. The above considerations imply that the polarization curves of the PILs should exhibit two onset potentials for the observed cathodic current density *j*, indicating the two different kinetic domains: (i) a domain with a mixed interface and

diffusion control and (ii) a domain under diffusion control only, that is, a limiting current density. The onset potential is determined by the intersection of the tangent line from the rising current density and the baseline. The onset potentials U_{ons} of PILs measured at 120 °C are listed in Table 3. The polarization curves of [DEMSPA][HSA] exhibit the first onset potential at about 0.90 V (vs Pd-H) and the second at about 0.55 V (vs Pd-H). Thus, below 0.55 V (vs Pd-H), the ORR current density is only limited by the mass transport of O_2 from the bulk electrolyte to the electrode surface. In the case of [DESPA][HSA], a similar first onset potential is observed, with diffusion control already being reached at 0.71 V (vs Pd-H). The onset potentials of the [TfO]-based electrolytes, that is, [DEMSPA][TfO] and [DESPA][TfO], are lower than those of the [HSA]-based electrolytes. As the diffusional mass transport depends on the product $D_{O_2} \cdot c_{O_2}$, the limiting current density of all investigated PILs increases with rising temperature (see Figure 7a and 7c). At a potential of about 0.6 V (vs Pd-H), that is, under diffusion control, the PILs based on [TfO] anions generally achieve higher cathodic current densities compared to those based on [HSA] anions. At 120 °C and 0.6 V (vs Pd-H), the cathodic current density increases in the order [DEMSPA][HSA] < [DESPA][HSA] << [DEMSPA][TfO] < [DESPA][TfO] (see Figure S6). This correlates quite well to the experimentally observed trend of the $D_{O_2} \cdot c_{O_2}$ product ([DEMSPA][HSA] << [DESPA][HSA] < [DEMSPA][TfO] ≈ [DESPA][TfO]). At more positive potentials, that is, 0.8 V (vs Pd-H) and 120 °C, a mixed kinetic and diffusion control is present. The absolute cathodic current values are lower, but the order remains unchanged (see Figure S6). It should be kept in mind that the ORR onset potential as well as the ORR current may be influenced by hydroxide and oxide adsorbates formed on the platinum surface at potentials higher than 0.8 V vs RHE. Studies of the ORR on Pt (111) single crystals in acid solutions have shown that the adsorption of OH leads to site blocking and negative electronic effects.[66-67] It should, however, be noted that oxide

coverages well below one are generated in the potential range investigated here. In any case, both the onset potentials and kinetic currents must be interpreted with care when used as diagnostic tools.

With increasing temperature, the onset potential of hydrogen evolution reaction (HER) in the [HSA]-based PILs shifts to values higher than the equilibrium potential of the hydrogen electrode. This suggests that the observed current is not only due to the reduction of adsorbed protons but also may be caused by another process such as anion reduction. Bancroft et al. reported the electrolysis of the concentrated sulfuric acid. They found that a mixture of hydrogen, hydrogen sulfide, and even sulfur can be formed by the reduction of sulfuric acid on Pt at temperatures higher than 80 °C.[68] However, a detailed analysis of this process is beyond the scope of this work and will be part of a future study.

Table 3 Onset Potential and Its Corresponded Current Density Measured at 120 °C of the PILs

PILs	onset potential U_{ons} (V)	current density j at U_{ons} (mA cm^{-2})	onset potential under diffusional control U_{lim} (V)	current density at U_{lim} (mA cm^{-2})
[DEMSPA][HSA]	0.90	-0.001	0.55	-0.015
[DEMSPA][TfO]	0.87	-0.006	0.56	-0.054
[DESPA][HSA]	0.93	-0.002	0.71	-0.020
[DESPA][TfO]	0.84	-0.012	0.62	-0.079

(a)

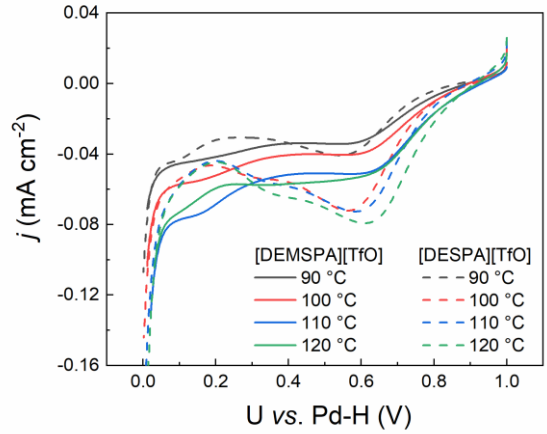
0.04
0.00
-0.04
-0.08
-0.12
-0.16
j (mA cm-2)
[DEMSPA][TfO]
90 °C
100 °C
110 °C
120 °C
[DESPA][TfO]
90 °C
100 °C
110 °C
120 °C
0.0
0.2
0.4
0.6
0.8
1.0
U vs. Pd-H (V)

(b)

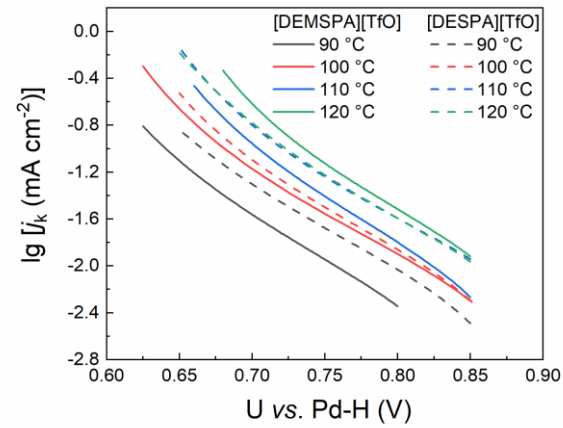
0.0
-0.4
-0.8
-1.2
-1.6
-2.0
-2.4
-2.8
lg [jk (mA cm-2)]
[DEMSPA][TfO]
90 °C
100 °C
110 °C
120 °C
[DESPA][TfO]
90 °C
100 °C
110 °C
120 °C
0.60
0.65
0.70
0.75
0.80
0.85
0.90
U vs. Pd-H (V)

(c)

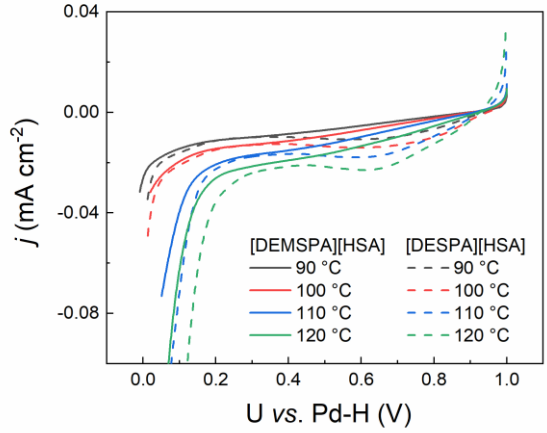
0.04
0.00
-0.04
-0.08
j (mA cm-2)
[DEMSPA][HSA]
90 °C
100 °C
110 °C
120 °C
[DESPA][HSA]
90 °C
100 °C
110 °C
120 °C
0.0
0.2
0.4
0.6
0.8
1.0
U vs. Pd-H (V)

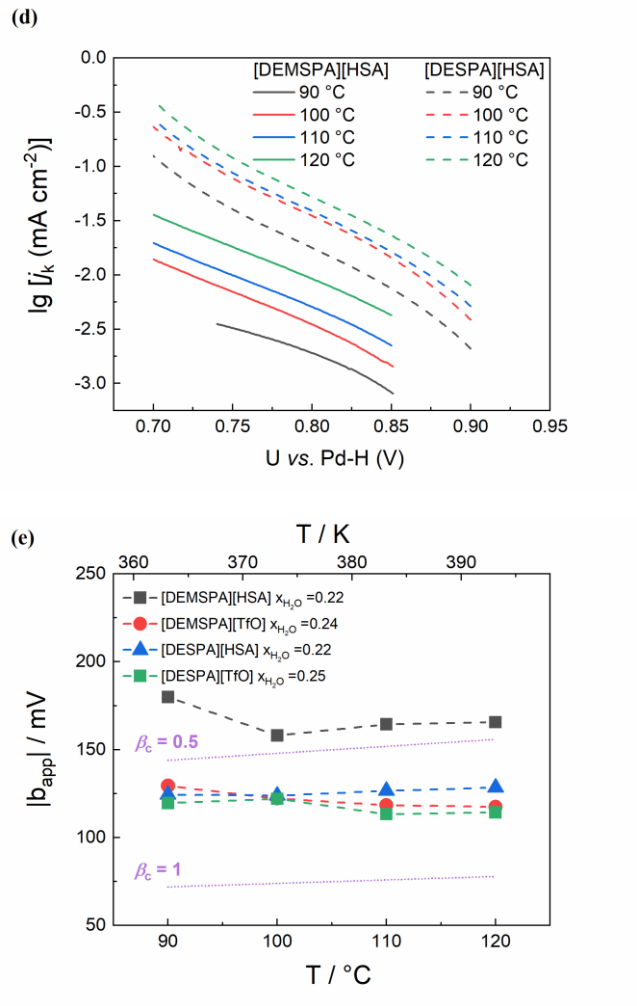

Figure 7. (a) ORR polarization curves and (b) mass-transport-corrected ORR Tafel plots for the Pt electrode in [TfO]-based PILs. (c) ORR polarization curves and (d) mass-transport-corrected ORR Tafel plots for the Pt electrode in [HSA]-based PILs. (e) Plots of Tafel factors |b_{app}| vs T, calculated from mass-transport-corrected Tafel plots by linear fitting. Here the dashed lines are just visual guids, not fits.

To compare the kinetic current densities, mass-transport-corrected current densities j_k are calculated according to eq 2. The corresponding Tafel plots are depicted in Figure 7b and 7d. As expected, j_k increases with rising temperature as the ORR is a thermally activated process. At a potential of 0.8 V (vs Pd-H) and 120 °C, the highest kinetic current density of 0.053 mA cm^{-2} is

achieved with [DESPA][HSA] (see Figure 7b and 7d). Under the same conditions, the other PILs yield values of 0.031 mA cm^{-2} ([DESPA][TfO]), 0.026 mA cm^{-2} ([DEMSPA][TfO]), and 0.009 mA cm^{-2} ([DEMSPA][HSA]). Assuming the ideal Butler-Volmer behavior of the kinetic current density, j_k should depend on the oxygen concentration at the electrode surface. A high O_2 solubility (c_{O_2}) should lead to a higher oxygen coverage on the Pt surface. Another parameter that has a strong influence on the ORR rate is the specific adsorption of anions on the Pt electrode surface.[69] It is shown in the literature that [HSA] anions form a thin adsorption layer on the surface of Pt.[70-71] This leads to a blockage of active sites and thus to a drop in the ORR rate.[72-73] The interaction of [TfO] anions with active sites on a Pt surface is much weaker compared to [HSA] anions.[74] The O_2 solubility (c_{O_2}) in the investigated PILs decreases in the order [DEMSPA][TfO] >> [DESPA][TfO] > [DESPA][HSA] > [DEMSPA][HSA]. This and the stronger interaction of the [HSA] anions with active sites may explain the very small kinetic current density (j_k) of [DEMSPA][HSA] but does not correlate with the j_k values for the other PILs. A conclusive explanation for the outstanding ORR kinetic performance of the [DESPA][HSA] cannot be given. Different hygroscopicity, loss of water at high temperatures, and water accumulation in the double-layer region might play a role. In fact, residual water could have a beneficial impact on the ORR kinetics, as it forms proton-donating H_3O^+ ions and modifies the double-layer structure, as well as the surface coverage of adsorbed species on the Pt surface.[75-76] However, these considerations are fairly speculative, and further investigations are still necessary.

According to eq 4, a linear, positive correlation between the temperature and the intrinsic factor $|b_{int}|$ can be expected. Using eq 3, a linear fitting of the slope of the $\log j_k - U$(Pd-H) curves in Figure 7b and 7d yield the apparent factor $|b_{app}|$ reported in Figure 7e. However, the experimental values $|b_{app}|$ differ from the calculated intrinsic factors $|b_{int}|$ (see broken lines in Figure 7e).

According to eq 3, this deviation can be explained by a change of $\mathrm{d}\theta_{ox}/\mathrm{d}U$ or θ_{ox} or β_c rather than in the reaction mechanism. The measured b_{app} value is more an indicator of the dynamic changing on the Pt surface coverage. Conway et al. have proposed several factors that can contribute to the changing of the symmetry factor β_c, for example, changes in the compact double-layer structure with temperature and potential, changes in the symmetry of the potential energy barrier, and the potential-dependent reactant adsorption.[77-78] Moreover, the deviation between the measured and theoretical Tafel slopes could also be caused by the impurities.[79] As an example, Scharifker et al. have stated that impurities in concentrated H_3PO_4 cause the changed behavior of the temperature dependence of the Tafel slope for ORR on Pt.[14]

4. CONCLUSION

In this study, N,N-diethyl-N-methyl-3-sulfopropan-1-ammonium hydrogen sulfate ([DEMSPA][HSA]), N,N-diethyl-N-methyl-3-sulfopropan-1-ammonium triflate ([DEMSPA][TfO]), N,N-diethyl-3-sulfopropan-1-ammonium hydrogen sulfate ([DESPA][HSA]), and N,N-diethyl-3-sulfopropan-1-ammonium triflate ([DESPA][TfO]) with a water molar fraction ranging from 0.22 to 0.29 were prepared. No crystallization phenomena are observed for all four PILs across a wide temperature range. The ionic conductivity of these electrolytes obeys the VFT equation. Their low conductivity at near room temperature can be interpreted by the high degree of ion pairing and the existence of a network of strong hydrogen bonds.

Nonetheless, the [TfO]-based PILs appear to offer better performance in IT-PEFC applications than the [HSA]-based ones. In fact, they provide the best combination of the fast ORR kinetics and fast oxygen transport, which is relevant for fuel cell operation. This applies in particular to [DESPA][TfO], which provides good ORR kinetics and fast oxygen transport (*i.e.*, the highest product of oxygen diffusivity and concentration), together with a high (total) ionic conductivity.

Moreover, it shows superior performance, especially at higher overpotentials. These features make [DESPA][TfO] a promising candidate for IT-PEFC applications.

ASSOCIATED CONTENT

Supporting Information

VFT-fitted temperature dependence of the viscosities of PILs, Arrhenius fitted dynamic viscosity of the PILs, VFT-fitted temperature dependence of the specific conductivities of PILs, Arrhenius fitted temperature dependence of the specific conductivities of PILs, Walden plot of the PILs, Cathodic current density measured at 0.6 V and 0.8 V, 120 °C of PILs.

AUTHOR INFORMATION

Corresponding Author

Carsten Korte

E-mail: c.korte@fz-juelich.de

Stefano Passerini

E-mail: stefano.passerini@kit.edu

Author Contributions

H.H. designed and performed the most experiments. H.M.S. performed thermal analysis under an air atmosphere. G.X. prepared the ionic liquids. All authors contributed to the results and discussion and revised the final manuscript. A.M., H.M.S., and K.W. had a great impact on the revision of the manuscript. C.K. and S.P. provided funding for the work.

Notes

The authors declare no competing financial interest.

ACKNOWLEDGMENT

H.H., H.M.S., A.M., and X.G. acknowledge the financial support of the Federal Ministry for Economic Affairs and Energy (HiFi-PEFC, Project 03ETB003A). H.H. acknowledges Dr. Thomas Schubert from Iolitec GmbH for the valuable suggestions in PIL synthesis. All authors are grateful for the support of the Helmholtz Association.

REFERENCES

(1) Li, Q.; He, R.; Jensen, J. O.; Bjerrum, N. J. Approaches and recent development of polymer electrolyte membranes for fuel cells operating above 100 C. *Chemistry of materials* **2003,** *15* (26), 4896-4915.

(2) Oetjen, H. F.; Schmidt, V.; Stimming, U.; Trila, F. Performance data of a proton exchange membrane fuel cell using H 2/CO as fuel gas. *Journal of the Electrochemical Society* **1996,** *143* (12), 3838-3842.

(3) Wilson, M.; Valerio, J.; Gottesfeld, S. In *Endurance testing of low Pt loading polymer electrolyte fuel cells*, Proceedings of the Symposium on Electrode Materials and Processes for Energy Conversion and Storage, The Electrochemical Society: 1994; p 145.

(4) Wainright, J.; Wang, J. T.; Weng, D.; Savinell, R.; Litt, M. Acid-doped polybenzimidazoles: a new polymer electrolyte. *Journal of the electrochemical society* **1995,** *142* (7), L121.

(5) Habib, M.; Bockris, J. In situ FT-IR spectroscopic study of electrochemical adsorption of phosphoric acid on platinum. *Electrochemical Society, Journal* **1983,** *130*, 2510-2512.

(6) Sacca, A.; Gatto, I.; Carbone, A.; Pedicini, R.; Passalacqua, E. ZrO2–Nafion composite membranes for polymer electrolyte fuel cells (PEFCs) at intermediate temperature. *Journal of power sources* **2006,** *163* (1), 47-51.

(7) Branco, C. M.; Sharma, S.; de Camargo Forte, M. M.; Steinberger-Wilckens, R. New approaches towards novel composite and multilayer membranes for intermediate temperature-polymer electrolyte fuel cells and direct methanol fuel cells. *Journal of Power Sources* **2016,** *316*, 139-159.

(8) Yasuda, T.; Watanabe, M. Protic ionic liquids: fuel cell applications. *MRS bulletin* **2013,** *38* (7), 560-566.

(9) Noda, A.; Hayamizu, K.; Watanabe, M. Pulsed-gradient spin− echo 1H and 19F NMR ionic diffusion coefficient, viscosity, and ionic conductivity of non-chloroaluminate room-temperature ionic liquids. *The Journal of Physical Chemistry B* **2001,** *105* (20), 4603-4610.

(10) Huang, X.-J.; Rogers, E. I.; Hardacre, C.; Compton, R. G. The reduction of oxygen in various room temperature ionic liquids in the temperature range 293− 318 K: Exploring the applicability of the Stokes− Einstein relationship in room temperature ionic liquids. *The Journal of Physical Chemistry B* **2009,** *113* (26), 8953-8959.

(11) Korte, C.; Conti, F.; Wackerl, J.; Lehnert, W. Phosphoric acid and its interactions with polybenzimidazole-type polymers. In *High Temperature Polymer Electrolyte Membrane Fuel Cells*; Springer: 2016; pp 169-194.

(12) Battino, R.; Rettich, T. R.; Tominaga, T. The solubility of oxygen and ozone in liquids. *Journal of physical and chemical reference data* **1983,** *12* (2), 163-178.

(13) Han, P.; Bartels, D. M. Temperature dependence of oxygen diffusion in H 2 O and D 2 O. *The Journal of physical chemistry* **1996,** *100* (13), 5597-5602.

(14) Scharifker, B. R.; Zelenay, P.; Bockris, J. M. The kinetics of oxygen reduction in molten phosphoric acid at high temperatures. *Journal of the Electrochemical Society* **1987,** *134* (11), 2714-2725.

(15) Takamura, Y.; Nakashima, E.; Yamada, H.; Tasaka, A.; Inaba, M. Effects of temperature and relative humidity on oxygen permeation in Nafion® and sulfonated poly (Arylene Ether Sulfone). *ECS Transactions* **2008,** *16* (2), 881.

(16) Mamlouk, M.; Scott, K. Phosphoric acid-doped electrodes for a PBI polymer membrane fuel cell. *International Journal of Energy Research* **2011,** *35* (6), 507-519.

(17) Liu, Z.; Wainright, J. S.; Litt, M. H.; Savinell, R. F. Study of the oxygen reduction reaction (ORR) at Pt interfaced with phosphoric acid doped polybenzimidazole at elevated temperature and low relative humidity. *Electrochimica Acta* **2006,** *51* (19), 3914-3923.

(18) Freemantle, M. *An introduction to ionic liquids*, Royal Society of chemistry: 2010.

(19) Wasserscheid, P.; van Hal, R.; Bösmann, A. 1-n-Butyl-3-methylimidazolium ([bmim]) octylsulfate—an even 'greener'ionic liquid. *Green Chemistry* **2002,** *4* (4), 400-404.

(20) Wippermann, K.; Wackerl, J.; Lehnert, W.; Huber, B.; Korte, C. 2-Sulfoethylammonium trifluoromethanesulfonate as an ionic liquid for high temperature PEM fuel cells. *Journal of The Electrochemical Society* **2016,** *163* (2), F25-F37.

(21) Nakamoto, H.; Watanabe, M. Bronsted acid-base ionic liquids for fuel cell electrolytes. *Chem Commun (Camb)* **2007,** (24), 2539-41, DOI: 10.1039/b618953a.

(22) Miran, M. S.; Yasuda, T.; Tatara, R.; Susan, M. A. B. H.; Watanabe, M. Amphoteric water as acid and base for protic ionic liquids and their electrochemical activity when used as fuel cell electrolytes. *Faraday discussions* **2017,** *206*, 353-364.

(23) Miran, M. S.; Yasuda, T.; Susan, M. A. B. H.; Dokko, K.; Watanabe, M. Electrochemical properties of protic ionic liquids: correlation between open circuit potential for H 2/O 2 cells under non-humidified conditions and Δp K a. *RSC Advances* **2013,** *3* (13), 4141-4144.

(24) Lee, S.-Y.; Ogawa, A.; Kanno, M.; Nakamoto, H.; Yasuda, T.; Watanabe, M. Nonhumidified intermediate temperature fuel cells using protic ionic liquids. *Journal of the American Chemical Society* **2010,** *132* (28), 9764-9773.

(25) Pan, H.; Geysens, P.; Putzeys, T.; Gennaro, A.; Yi, Y.; Li, H.; Atkin, R.; Binnemans, K.; Luo, J.; Wübbenhorst, M. Physicochemical study of diethylmethylammonium methanesulfonate under anhydrous conditions. *The Journal of chemical physics* **2020,** *152* (23), 234504.

(26) Noda, A.; Susan, M. A. B. H.; Kudo, K.; Mitsushima, S.; Hayamizu, K.; Watanabe, M. Brønsted acid− base ionic liquids as proton-conducting nonaqueous electrolytes. *The Journal of Physical Chemistry B* **2003,** *107* (17), 4024-4033.

(27) Khan, A.; Lu, X.; Aldous, L.; Zhao, C. Oxygen reduction reaction in room temperature protic ionic liquids. *The Journal of Physical Chemistry C* **2013,** *117* (36), 18334-18342.

(28) Johnson, L.; Ejigu, A.; Licence, P.; Walsh, D. A. Hydrogen oxidation and oxygen reduction at platinum in protic ionic liquids. *The Journal of Physical Chemistry C* **2012,** *116* (34), 18048-18056.

(29) Zhao, C.; Bond, A. M.; Lu, X. Determination of water in room temperature ionic liquids by cathodic stripping voltammetry at a gold electrode. *Analytical chemistry* **2012,** *84* (6), 2784-2791.

(30) Compañ, V.; Escorihuela, J.; Olvera, J.; García-Bernabé, A.; Andrio, A. Influence of the anion on diffusivity and mobility of ionic liquids composite polybenzimidazol membranes. *Electrochimica Acta* **2020,** *354*, 136666.

(31) Le Bideau, J.; Viau, L.; Vioux, A. Ionogels, ionic liquid based hybrid materials. *Chemical Society Reviews* **2011,** *40* (2), 907-925.

(32) Angell, C. A.; Byrne, N.; Belieres, J.-P. Parallel developments in aprotic and protic ionic liquids: Physical chemistry and applications. *Accounts of chemical research* **2007,** *40* (11), 1228-1236.

(33) Zhu, Z.; Yan, X.; Tang, H.; Cai, H.; Pan, M.; Zhang, H.; Luo, J. Protic ionic liquid modified electrocatalyst enables robust anode under cell reversal condition. *Journal of Power Sources* **2017,** *351*, 138-144.

(34) Bao, X.; Zhang, F.; Liu, Q. Sulfonated poly (2, 5-benzimidazole)(ABPBI)/MMT/ionic liquids composite membranes for high temperature PEM applications. *international journal of hydrogen energy* **2015,** *40* (46), 16767-16774.

(35) Ye, H.; Huang, J.; Xu, J.; Kodiweera, N.; Jayakody, J.; Greenbaum, S. New membranes based on ionic liquids for PEM fuel cells at elevated temperatures. *Journal of Power Sources* **2008,** *178* (2), 651-660.

(36) Bernal-López, M.; Selva-Ochoa, A.; Borja-Arco, E.; Magallón-Cacho, L.; Su-Gallegos, J. Microwave assisted synthesis of metallic Ru for the HOR and ORR. *Materials Research Express* **2020,** *7* (2), 025503.

(37) Malko, D.; Lopes, T.; Symianakis, E.; Kucernak, A. The intriguing poison tolerance of non-precious metal oxygen reduction reaction (ORR) catalysts. *Journal of Materials Chemistry A* **2016,** *4* (1), 142-152.

(38) Debe, M. K. Electrocatalyst approaches and challenges for automotive fuel cells. *Nature* **2012,** *486* (7401), 43-51.

(39) Reimer, U.; Ehlert, J.; Janßen, H.; Lehnert, W. Water distribution in high temperature polymer electrolyte fuel cells. *International journal of hydrogen energy* **2016,** *41* (3), 1837-1845.

(40) Schultze, J.; Wippermann, K. Inhibition of electrode processes on copper by AHT in acid solutions. *Electrochimica Acta* **1987,** *32* (5), 823-831.

(41) Gottesfeld, S. Some observations on the oxygen reduction reaction (ORR) at platinum catalysts based on post year 2000 reports. *ECS Transactions* **2008,** *6* (25), 51-67.

(42) Pasti, I. A.; Gavrilov, N. M.; Mentus, S. V. Potentiodynamic investigation of oxygen reduction reaction on polycrystalline platinum surface in acidic solutions: The effect of the polarization rate on the kinetic parameters. *Int. J. Electrochem. Sci* **2012,** *7*, 11076-11090.

(43) Guidelli, R.; Compton, R. G.; Feliu, J. M.; Gileadi, E.; Lipkowski, J.; Schmickler, W.; Trasatti, S. Defining the transfer coefficient in electrochemistry: An assessment (IUPAC Technical Report). *Pure and Applied Chemistry* **2014,** *86* (2), 245-258, DOI: 10.1515/pac-2014-5026.

(44) Shoup, D.; Szabo, A. Chronoamperometric current at finite disk electrodes. *Journal of Electroanalytical Chemistry and Interfacial Electrochemistry* **1982,** *140* (2), 237-245.

(45) Makhlooghiazad, F.; Guazzagaloppa, J.; O'Dell, L. A.; Yunis, R.; Basile, A.; Howlett, P. C.; Forsyth, M. The influence of the size and symmetry of cations and anions on the physicochemical behavior of organic ionic plastic crystal electrolytes mixed with sodium salts. *Physical Chemistry Chemical Physics* **2018,** *20* (7), 4721-4731.

(46) Gardas, R. L.; Freire, M. G.; Carvalho, P. J.; Marrucho, I. M.; Fonseca, I. M.; Ferreira, A. G.; Coutinho, J. A. High-pressure densities and derived thermodynamic properties of imidazolium-based ionic liquids. *Journal of Chemical & Engineering Data* **2007,** *52* (1), 80-88.

(47) Gomes de Azevedo, R.; Esperança, J. M.; Najdanovic-Visak, V.; Visak, Z. P.; Guedes, H. J.; Nunes da Ponte, M.; Rebelo, L. P. Thermophysical and thermodynamic properties of 1-butyl-3-methylimidazolium tetrafluoroborate and 1-butyl-3-methylimidazolium hexafluorophosphate over an extended pressure range. *Journal of Chemical & Engineering Data* **2005,** *50* (3), 997-1008.

(48) Elia, G. A.; Ulissi, U.; Mueller, F.; Reiter, J.; Tsiouvaras, N.; Sun, Y. K.; Scrosati, B.; Passerini, S.; Hassoun, J. A Long-Life Lithium Ion Battery with Enhanced Electrode/Electrolyte Interface by Using an Ionic Liquid Solution. *Chemistry–A European Journal* **2016,** *22* (20), 6808-6814.

(49) Gao, X.; Wu, F.; Mariani, A.; Passerini, S. Concentrated Ionic-Liquid-Based Electrolytes for High-Voltage Lithium Batteries with Improved Performance at Room Temperature. *ChemSusChem* **2019,** *12* (18), 4185-4193.

(50) Elia, G. A.; Ulissi, U.; Jeong, S.; Passerini, S.; Hassoun, J. Exceptional long-life performance of lithium-ion batteries using ionic liquid-based electrolytes. *Energy & Environmental Science* **2016,** *9* (10), 3210-3220.

(51) Lin, J.; Wang, L.; Zinkevich, T.; Indris, S.; Suo, Y.; Korte, C. Influence of residual water and cation acidity on the ionic transport mechanism in proton-conducting ionic liquids. *Physical Chemistry Chemical Physics* **2020,** *22* (3), 1145-1153.

(52) Schreiner, C.; Zugmann, S.; Hartl, R.; Gores, H. J. Fractional Walden rule for ionic liquids: examples from recent measurements and a critique of the so-called ideal KCl line for the Walden plot. *Journal of Chemical & Engineering Data* **2009,** *55* (5), 1784-1788.

(53) MacFarlane, D. R.; Forsyth, M.; Izgorodina, E. I.; Abbott, A. P.; Annat, G.; Fraser, K. On the concept of ionicity in ionic liquids. *Physical Chemistry Chemical Physics* **2009,** *11* (25), 4962-4967.

(54) Zhao, Y. H.; Abraham, M. H.; Zissimos, A. M. Fast calculation of van der Waals volume as a sum of atomic and bond contributions and its application to drug compounds. *The Journal of organic chemistry* **2003,** *68* (19), 7368-7373.

(55) Edward, J. T. Molecular volumes and the Stokes-Einstein equation. *Journal of Chemical Education* **1970,** *47* (4), 261.

(56) Mariani, A.; Bonomo, M.; Wu, B.; Centrella, B.; Dini, D.; Castner, E. W.; Gontrani, L. Intriguing transport dynamics of ethylammonium nitrate–acetonitrile binary mixtures arising from nano-inhomogeneity. *Physical Chemistry Chemical Physics* **2017,** *19* (40), 27212-27220.

(57) Neale, A. R.; Li, P.; Jacquemin, J.; Goodrich, P.; Ball, S. C.; Compton, R. G.; Hardacre, C. Effect of cation structure on the oxygen solubility and diffusivity in a range of bis {(trifluoromethyl) sulfonyl} imide anion based ionic liquids for lithium–air battery electrolytes. *Physical Chemistry Chemical Physics* **2016,** *18* (16), 11251-11262.

(58) Wesseler, E. P.; Iltis, R.; Clark Jr, L. C. The solubility of oxygen in highly fluorinated liquids. *Journal of Fluorine Chemistry* **1977,** *9* (2), 137-146.

(59) Gui, A. L.; Endres, F.; Wittstock, G. Influence of Chemical Structure and Temperature on Oxygen Reduction Reaction and Transport in Ionic Liquids. *Zeitschrift für Physikalische Chemie* **2017,** *231* (6), 1077.

(60) Anthony, J. L.; Maginn, E. J.; Brennecke, J. F. Solubilities and thermodynamic properties of gases in the ionic liquid 1-n-butyl-3-methylimidazolium hexafluorophosphate. *The Journal of Physical Chemistry B* **2002,** *106* (29), 7315-7320.

(61) Lei, Z.; Dai, C.; Chen, B. Gas solubility in ionic liquids. *Chemical reviews* **2014,** *114* (2), 1289-1326.

(62) Kumełan, J.; Kamps, Á. P.-S.; Urukova, I.; Tuma, D.; Maurer, G. Solubility of oxygen in the ionic liquid [bmim][PF6]: Experimental and molecular simulation results. *The Journal of Chemical Thermodynamics* **2005,** *37* (6), 595-602.

(63) Huang, J.; Sen, R.; Yeager, E. Oxygen reduction on platinum in 85% orthophosphoric acid. *Journal of The Electrochemical Society* **1979,** *126* (5), 786.

(64) Walsh, D. A.; Ejigu, A.; Smith, J.; Licence, P. Kinetics and mechanism of oxygen reduction in a protic ionic liquid. *Physical Chemistry Chemical Physics* **2013,** *15* (20), 7548-7554.

(65) Wippermann, K.; Suo, Y.; Korte, C. Suitability of the Hanging Meniscus RDE for the Electrochemical Investigation of Ionic Liquids. *Journal of The Electrochemical Society* **2020,** *167* (4), 046511.

(66) Wang, J. X.; Markovic, N. M.; Adzic, R. R. Kinetic Analysis of Oxygen Reduction on Pt(111) in Acid Solutions: Intrinsic Kinetic Parameters and Anion Adsorption Effects. *The Journal of Physical Chemistry B* **2004,** *108* (13), 4127-4133, DOI: 10.1021/jp037593v.

(67) Wang, J. X.; Zhang, J.; Adzic, R. R. In *What matters after first electron transfer in oxygen reduction: A kinetic study of Pt(111) and Pt/C thin layer catalysts on rotating disk electrodes*, ACS Division of Fuel Chemistry, Preprints, 2004; pp 664-665.

(68) Bancroft, W. D.; Magoffin, J. E. Energy Levels in Electrochemistry. *Journal of the American Chemical Society* **1935,** *57* (12), 2561-2565.

(69) Teliska, M.; Murthi, V. S.; Mukerjee, S.; Ramaker, D. E. Site-specific vs specific adsorption of anions on Pt and Pt-based alloys. *The Journal of Physical Chemistry C* **2007,** *111* (26), 9267-9274.

(70) Zelenay, P.; Wieckowski, A.; Abruna, H. Modern techniques for in situ surface characterization. In *Electrochemical Interfaces*; VCH Publishers New York: 1991.

(71) Kolics, A.; Wieckowski, A. Adsorption of bisulfate and sulfate anions on a Pt (111) electrode. *The Journal of Physical Chemistry B* **2001,** *105* (13), 2588-2595.

(72) Perez, J.; Villullas, H. M.; Gonzalez, E. R. Structure sensitivity of oxygen reduction on platinum single crystal electrodes in acid solutions. *Journal of Electroanalytical Chemistry* **1997,** *435* (1-2), 179-187.

(73) Marković, N.; Adžić, R.; Cahan, B.; Yeager, E. Structural effects in electrocatalysis: oxygen reduction on platinum low index single-crystal surfaces in perchloric acid solutions. *Journal of Electroanalytical Chemistry* **1994,** *377* (1-2), 249-259.

(74) Furuya, Y.; Mashio, T.; Ohma, A.; Dale, N.; Oshihara, K.; Jerkiewicz, G. Surface oxide growth on platinum electrode in aqueous trifluoromethanesulfonic acid. *The Journal of chemical physics* **2014,** *141* (16), 164705.

(75) Wippermann, K.; Giffin, J.; Korte, C. In Situ determination of the water content of ionic liquids. *Journal of The Electrochemical Society* **2018,** *165* (5), H263-H270.

(76) Wippermann, K.; Giffin, J.; Kuhri, S.; Lehnert, W.; Korte, C. The influence of water content in a proton-conducting ionic liquid on the double layer properties of the Pt/PIL interface. *Physical Chemistry Chemical Physics* **2017,** *19* (36), 24706-24723.

(77) Clouser, S.; Huang, J.; Yeager, E. Temperature dependence of the Tafel slope for oxygen reduction on platinum in concentrated phosphoric acid. *Journal of applied electrochemistry* **1993,** *23* (6), 597-605.

(78) Conway, B.; Bockris, J. O. M.; White, R. E. *Modern Aspects of Electrochemistry: No. 13*, Springer: 1979.

(79) Hibino, T.; Akimoto, T.; Iwahara, H. Protonic conduction of mordenite-type zeolite. *Solid State Ionics* **1993,** *67* (1-2), 71-76.

Table of contents